Available online at www.sciencedirect.com
ScienceDirect
Journal of the European Ceramic Society 28 (2008) 747–756
www.elsevier.com/locate/jeurceramsoc

Phase formation of $CaAl_2O_4$ from $CaCO_3$–Al_2O_3 powder mixtures

Shahriar Iftekhar[a], Jekabs Grins[a,*], Gunnar Svensson[a], Jesper Lööf[b], Tobias Jarmar[b], Gianluigi A. Botton[c], Carmen M. Andrei[c], Håkan Engqvist[d]

[a] *Department of Physical, Inorganic and Structural Chemistry, Arrhenius Laboratory, Stockholm University, S-106 91 Stockholm, Sweden*
[b] *Doxa AB, Axel Johanssons gata 4-6, S-754 51 Uppsala, Sweden*
[c] *Brockhouse Institute for Materials Research, McMaster University, Hamilton, ON L8S 4M1, Canada*
[d] *Department of Engineering Sciences, Box 534, The Angstrom Laboratory, Uppsala University, 751 21 Uppsala, Sweden*

Received 5 June 2007; accepted 22 August 2007
Available online 19 November 2007

Abstract

Calcium aluminate is the main constituent in calcium aluminate cements, used in a wide range of applications in construction and mining industries and recently also as biomedical implant. In applications that demand very precise reaction features, such as the biomedical ones, the phase purity is of very high importance.

In this paper the formation of $CaAl_2O_4$ from $CaCO_3$–Al_2O_3 powder mixtures has been studied, varying holding times between 1 and 40 h and temperatures between 1300 and 1500 °C. Phase formation was studied in samples both quenched from the holding temperatures and in samples slowly cooled. Samples were characterized by X-ray powder diffraction (XRPD), using Guinier-Hägg film data and the Rietveld method, and scanning (SEM) and transmission (TEM) electron microscopy. Samples for TEM with very high site accuracy were produced using focused ion beam microscopy.

In addition to CA ($CaAl_2O_4$) the samples contained major amounts of CA_2 ($CaAl_4O_7$), $C_{12}A_7$ ($Ca_{12}Al_{14}O_{33}$) and minor amounts of un-reacted A (Al_2O_3). Trace amounts of C_3A ($Ca_3Al_2O_6$) were observed only for samples heated to 1500 °C. The amount of the Ca-rich phase $C_{12}A_7$ was found to decrease with time as it reacts with A and, to a less degree, CA_2 to form CA. In agreement with previous studies the amount of CA_2 formed decreases comparatively slowly with time. Its un-reactivity is due to that it is concentrated in isolated porous regions of sizes up to 100 μm. The formation of the Ca aluminates is found to be in response to local equilibriums within small inhomogeneous regions, with no specific phase acting as an intermediate phase. Samples quenched from 1500 °C were found to contain smaller amounts of poorly crystallized phases. A reaction between C and A takes place already at 900 °C, forming a meta-stable orthorhombic modification of CA. The orthorhombic unit cell with $a = 8.732(2)$ Å, $b = 8.078(2)$ Å, $c = \sqrt{3} \cdot a = 15.124(4)$ Å was verified by electron diffraction, revealing frequent twinning and disorder of the crystallites.

Keywords: Calcium aluminates; Calcinations; Powders-solid state reaction; Microstructure; Alkaline earth oxides; Al_2O_3; $CaAl_2O_4$

1. Introduction

The C–A (CaO–Al_2O_3) phase diagram has been determined by Chatterjee and Zhmoidin[1] and contains the phases A, CA_6, CA_2, CA, $C_{12}A_7$, C_3A and C. CA melts congruently at 1600 °C and there is an eutectic at 1390 °C for 47.5 wt% CaO. This phase diagram is relevant only in ambient air that contains moisture and under dry conditions the phase $C_{12}A_7$ does not form. The phase diagram in a moisture free atmosphere has been determined by Nurse et al.[2] and later assessed by Hallstedt[3] and Eriksson et al.[4] However, this phase diagram does not contain the orthorhombic phase C_5A_3, which forms in very dry air or nitrogen atmosphere.[5] Standard Gibbs free energies for the formation of the Ca aluminates have been determined by Rog et al.[6]

CA is the main constituent in calcium alumina cements, used in a wide range of applications in construction and mining industries. Doped with Eu^{2+} it shows persistent luminescence and is therefore potentially applicable in radiation detectors, sensors for structural damage and temperature, as well as luminous paints.[7,8] Recently, it has found application as a precursor for bioceramics in teeth[9] and spine. These show very good biocompatibility with the skeletal forming phases in the body,[10] *e.g.* apatite. A meta-stable form of $CaAl_2O_4$ is obtained upon

* Corresponding author. Tel.: +46 8 161254; fax: +46 8 152187.
E-mail address: mat@inorg.su.se (J. Grins).

0955-2219/$ – see front matter © 2007 Elsevier Ltd. All rights reserved.
doi:10.1016/j.jeurceramsoc.2007.08.012

synthesis at lower temperatures (850–1000 °C), *e.g.* by sol–gel methods.[8,11,12] Its crystal structure has not been solved in detail and the unit cell has been proposed as being orthorhombic ($a = 8.74$ Å, $b = 8.10$ Å, $c = 15.13$ Å, PDF No. 33-0252) or hexagonal ($a = 8.74$ Å, $c = 8.08$ Å, space group $P6_3$, $Z = 6$).[12] When used as a cement, *i.e.* mixed with water to a paste and let to harden, CA converts mainly into stable katoite ($Ca_3Al_2(OH)_{12}$) and gibbsite ($Al(OH)_3$).[13]

Because of their industrial importance, the phase formation of Ca aluminates has been the subject of several studies. Although most studies are in agreement in many respects, they also have led to different conclusions. Williamson and Glasser[14] concluded that for 1:1 mixtures of $CaCO_3$ and Al_2O_3, heated for 3–120 h at 1045–1405 °C, no specific phase is preferentially formed as a first, non-equilibrium reaction product. They were not able to determine diffusion mechanisms, as they regarded the samples to contain inhomogeneous regions that were very probably larger than the diffusing distance of ions. In a later study, Singh et al.[15] studied the formation kinetics in the temperature range 1200–1460 °C using mixtures of CaO and Al_2O_3. They found that all stable aluminates are formed in the beginning, but as the reaction proceeds, some disappear and the amounts of equilibrium phases increase. The lime-rich phases C_3A and $C_{12}A_7$ were found in the beginning of heat treatments at 1250 and 1300 °C and then decreased in amount with time. The observed proportion of CA_2 was small and decreased more slowly with time. Their conclusions were that lime-rich phases are formed quickly and then combine with alumina, and that CA in 1:1 mixtures is not formed by direct reaction between CaO and Al_2O_3 but proceeds by conversion of reaction intermediates. A further study was carried out by Mohamed and Sharpe,[16] at temperatures 1150–1400 °C and using mixtures of $CaCO_3$ and Al_2O_3. They concluded that their findings were in closer agreement with those of Williamson and Glasser, but also that C_3A and $C_{12}A_7$ are to be considered as intermediates in the formation of CA, whereas CA_2 is formed via an initial side reaction. In most investigations, dry-mixed mixtures of $CaCO_3$ and Al_2O_3 have been used as starting materials. Synthesis of CA by such a conventional method can be expected to yield non-equilibrium mixtures of phases and alternative syntheses routes have indeed been used to increase yields and/or shorten synthesis times; combustion synthesis,[17,18] spray-drying,[19] attrition milling,[20] the Pechini process,[21] and sol–gel methods.[22–27] These routes have, however, their disadvantages for larger-scale synthesis, in increased costs and increased number of steps in the synthesis.

The present study of CA formation was carried out in order to reassess previous studies, using the Rietveld method to quantify amounts of formed crystalline phases and electron microscopy to investigate micro-structures and reaction zones.

2. Experimental

To confirm the phase diagram, mono-phasic samples of the Ca aluminates CA_6, CA_2, CA, $C_{12}A_7$ and C_3A were prepared. For syntheses of these, corresponding mixtures were first tumbled with Al_2O_3 bodies in iso-propanol for 2 days and then in addition ground in hexane by hand. For heat treatments the powders were pressed into pellets using a pressure of *ca.* 50 MPa and the pellets placed inside a Pt crucible. The temperatures applied for syntheses of mono-phasic samples of the Ca aluminates are given below.

Table 1
Parameters varied during heat treatment

t_1 (h)	T_2 (°C)	t_2 (h)
1	1300	1
20	1400	4.5
40	1500	9

For the aimed studies of phase formation of CA, a dry-mixed 1:1 mixture of $CaCO_3$ and Al_2O_3 was used. The size of the $CaCO_3$ and Al_2O_3 grains was below 10 μm and below 1 μm, respectively. A programmable Nabertherm high-temperature furnace with $MoSi_2$ heating elements was used for the heating cycles. A total of twenty-two different heat treatments were applied for the dry-mix CA samples. A constant weight of 0.3465 grams was used for each pellet. They were first heated from 100 °C to $T_1 = 900$ °C at a rate of 5 °C/min and held there for different t_1 hours. The temperature was then increased at a rate of 5 °C/min to three different T_2 temperatures (1300, 1400, and 1500 °C) and held there for different t_2 hours. For $T_2 = 1300$ and 1500 °C the combinations of t_1 and t_2 were respectively (1, 40 h) and (1, 9 h), see Table 1. For $T_2 = 1400$ °C, three individual runs were made with $t_1 = 20$ h and $t_2 = 4.5$ h in order to check the reproducibility of the results. For each combination of t_1, t_2 and T_2, samples were either quenched from T_2, by rapidly withdrawing the Pt crucible from the furnace, or allowed to cool to 100 °C at the rate of 7 °C/min.

Guinier-Hägg films were recorded using a 50 mm camera, Cu $K\alpha_1$ radiation, and Si as internal standard. The films were read with a LS-20 film densitometer.[28] The Guinier-Hägg films were evaluated using the program SCANPI,[29] yielding intensity data on an arbitrary scale and the 2θ scale linearly corrected by the positions of the Si internal standard. Phase fractions of observed phases were determined from refined scale factors for the phases in Rietveld refinements, using the program FullProf[30] and data up to $2\theta = 85°$ with a flat background of 1000 added. Crystallographic data for the phases were taken from the ICSD[31] and PDF[32] data bases. Atomic coordinates for A, CA_2, CA, $C_{12}A_7$ and C_3A were taken from references,[33–37] respectively, and not refined. For $C_{12}A_7$, a full occupancy of atomic sites was assumed, and not the partially occupied ones proposed in reference,[36] corresponding to a composition of $C_{11.3}A_7$ (*c.f.* below). Thirty to 35 parameters were refined for each pattern, including; scale factors for the phases, unit cell parameters for the phases, a 0 point error, collective temperature factors for each phase (including an absorption contribution), a profile shape parameter (eta value for Pearson VII profile), two profile asymmetry parameters, parameters describing the dependence of reflection breadths with 2θ (U, V, W), and two to three polynomial coefficients for background.

The weight fraction of a phase j was estimated from

$$W_j = \frac{S_j Z_j M_j V_j}{\sum_i S_i Z_i M_i V_i}$$

where S is the (refined) scale factor, Z the number of formula units in unit cell, M the mass of formula unit, V the unit cell volume, and the sum over all phases i. The obtained estimated standard deviations for the weight fraction given below are not corrected for serial correlation, the factor proposed by the program being *ca.* 3. From the obtained phase fractions, the total Ca content, Ca_{tot}, relative to the total Al_2 content, *i.e.* $Ca_{tot} = 2 \times$ (total Ca/total Al) were also calculated. The latter was made as a check of the validity of the refinements and the value should not be far off from 1 for a CA mixture.

Samples for SEM were mounted using a low-viscosity epoxy resin (Buehler, EpoThin, 20-8140-032) and hardener (Buehler, 20-8142-016). The sample surfaces were polished flat in water-free ethylene glycol using 4000 mesh SiC papers, cleaned by ultra-sound in methanol, and carbon coated. SEM studies were made using a JEOL JSM-820 SEM, equipped with an AN10000 energy dispersive X-ray (EDX) micro-analysis system. TEM studies were made using a JEOL 2000FX and a JEOL 2010 F. Samples for TEM were produced using focused ion beam microscopy (FIB, Strata DB235). Preparation of TEM foils using FIB has been described in detail elsewhere.[38,39] In brief, FIB uses Ga^+ ions to either image or mill samples. Using the milling functions thin foils can be fabricated with a very site-specific accuracy (of the order of microns). The foils are normally in the order of 10 μm × 20 μm in size and have a thickness of about 100 nm.

3. Results

3.1. Synthesis of mono-phasic Ca aluminates

All compositions were first heated to 1350 °C at a rate of 5°/min and heat-treated for 24 h. This yielded mono-phasic samples of the Ca rich phases C_3A and $C_{12}A_7$. Refinements of phase fractions in the other samples by the Rietveld method showed the CA_6 sample to contain in addition 13(1) wt% A and 12(1) wt% CA_2, the CA_2 sample 0.5(2) wt% A and 2.5(4) wt% $C_{12}A_7$, and the CA sample 1.5(3) wt% CA_2 and 1.7(2) wt% $C_{12}A_7$. These samples were then re-ground and fired again at temperatures of respectively 1650, 1500 and 1400 °C for 24 h, yielding X-ray pure samples.

A structure determination of $C_{12}A_7$ from high-quality neutron powder diffraction data[36] asserts that the phase is Ca and O deficient and that its real composition is close to $C_{11.3}A_7$ (44.7% Ca instead of 46.2%). This was not observed here for the following reasons. First, a sample with composition $C_{11.3}A_7$ heat-treated in the same way contained in addition the neighbouring phase CA. Second, no shifts of Bragg reflections, indicative of a solubility range, could be observed. Third, EDX analysis in SEM on polished surfaces of the two samples yielded within error identical compositions, 46.4 at.% Ca.

3.2. Phase fractions in CA samples from Guinier-Hägg XRPD data

There were no difficulties to detect the presence of A, CA_2, CA and $C_{12}A_7$ and they were well suited for Rietveld refinements, see Fig. 1. The C_3A phase, whose presence during the formation of CA has been discussed in several reports, was only observed in one sample.

The results for samples heat-treated at 1400 °C are given in Table 2. No difference was observed between quenched, Q, samples and full run, FR, samples. The values validate the precision of the method, with the means and standard deviations of the phase fractions being 2(1) wt% A, 6(1) wt% CA_2, 77(2) wt% CA, and 15(1) wt% $C_{12}A_7$. The presence of minority phases, 0.1–0.5 wt%, could be confirmed by visual inspection of the films. Regrinding the samples and heat-treating them for a second FR resulted in a nearly phase pure CA sample, containing 0.4(2) wt% CA_2 and 4.6(2) wt% $C_{12}A_7$. Non-pelletized sam-

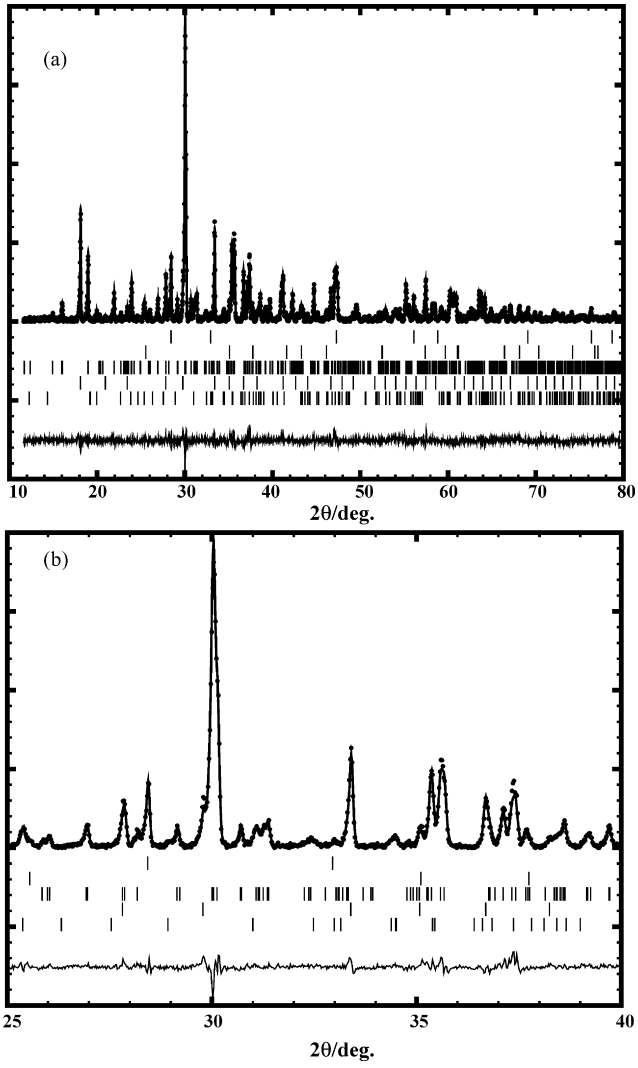

Fig. 1. Illustration of fit between observed and calculated XRPD intensities for (a) $2\theta = 10$–$80°$, (b) $2\theta = 25$–$40°$. Reflection markers are, from bottom up, for CA_2, $C_{12}A_7$, CA, A, and Si (internal standard).

Table 2
Determined amounts of crystalline phases in wt% for CA samples heat-treated at 1400 °C (t_1/t_2 = 20/4.5 h)

Sample	A	CA_2	CA	$C_{12}A_7$	Ca_{tot}
FR	2.3(2)	6.2(4)	77(1)	14.7(3)	1.01(2)
FR	3.0(1)	6.1(5)	75(1)	16.0(3)	1.01(2)
FR	2.3(2)	5.5(4)	77(1)	15.6(3)	1.02(2)
Q	0.8(1)	5.4(4)	81(1)	12.9(3)	1.02(2)
Q	1.8(2)	7.7(6)	76(1)	14.6(3)	1.01(2)
Q	2.0(2)	5.2(4)	78(1)	14.4(3)	1.02(2)

FR: full run and Q: quenched samples.

Table 3
Determined amounts of crystalline phases in wt% for samples heat-treated at 1300 °C

t_1/t_2	A	CA_2	CA	$C_{12}A_7$	Ca_{tot}
1/1 FR	13.4(6)	8.8(6)	42(1)	35.1(6)	0.93(2)
1/1 Q	11.3(6)	8.9(7)	43(1)	36.6(6)	0.98(3)
1/9 FR	5.8(4)	7.9(6)	65(1)	21.4(4)	0.98(2)
1/9 Q	6.0(3)	9.3(6)	66(1)	20.1(4)	0.97(2)
40/1 FR	14.7(6)	7.0(5)	42(1)	36.4(4)	0.94(2)
40/1 Q	12.2(9)	6.7(8)	45(1)	36.3(9)	0.98(3)
40/9 FR	5.9(4)	9.0(5)	64(1)	20.9(4)	0.97(2)
40/9 Q	7.4(6)	7.6(6)	63(1)	22.2(5)	0.97(2)

FR: full run and Q: quenched samples.

ples were also heat-treated, yielding no significant difference in obtained phase fractions.

The results for samples heat-treated at 1300 and 1500 °C are given in respectively Tables 3 and 4. The 1300 °C samples show, as the 1400 °C samples, no significant difference between Q and FR samples. As T_2 was decreased from 1400 to 1300 °C, the amounts of secondary phases increased; for A from *ca.* 1–2 wt% to 5–10 wt%, for CA_2 from *ca.* 5 wt% to 5–10 wt%, and for $C_{12}A_7$ from *ca.* 13 wt% to 20–40 wt%. The changes in the amounts of A and $C_{12}A_7$ were substantially larger than that for CA_2. The effect of varying t_1 can be seen by comparisons of t_1/t_2 = 1/1–40/1 and 1/9–40/9 samples. The conclusion is that varying t_1 has no effect on the phase fractions. The effect of varying t_2 can be seen by comparisons of t_1/t_2 = 1/1–1/9 and 40/1–40/9 samples. Samples with longer t_2 contained less A and $C_{12}A_7$, and consequently more CA, as the amount of CA_2 was not affected. This showed that, in the phase formation at 1300 °C, $C_{12}A_7$ reacts with primarily A, while CA_2 once formed is more un-reactive. This is in agreement with the findings in previous studies.

Table 4
Determined amounts of crystalline phases in wt% for samples heat-treated at 1500 °C

t_1/t_2	A	CA_2	CA	$C_{12}A_7$	C_3A	Ca_{tot}
1/1 FR	2.8(2)	7.2(4)	72(4)	17.9(3)	–	1.01(2)
1/1 Q	–	5.5(4)	91(1)	3.1(2)	–	0.98(2)
1/9 FR	–	7.0(4)	81(1)	11.8(3)	–	1.02(2)
1/9 Q	0.5(2)	8.0(7)	91(1)	0.2(2)	–	0.95(2)
40/1 FR	3.1(4)	7.4(4)	73(1)	16.4(5)	–	1.00(2)
40/1 Q	2.1(2)	7.0(5)	74(1)	16.7(3)	–	1.02(2)
40/9 FR	–	5.6(4)	91(2)	–	3.8(1)	1.01(2)
40/9 Q	–	7.3(6)	93(2)	0.1(2)	–	0.96(2)

FR: full run and Q: quenched samples.

The results for the 1500 °C samples are more difficult to interpret. Consistent interpretation of the results can be made if the quenched sample with t_1/t_2 = 40/1 h is disregarded. As for the other T_2, there is no significant effect of varying t_1. As for the 1400 °C series of samples, there are only small amounts of A. The amount of CA_2 is fairly constant, 7(1) wt% and is not decreased by increasing T_2 from 1400 to 1500 °C. The largest differences between the samples were in the fractions of $C_{12}A_7$. As t_2 was increased, the amounts of $C_{12}A_7$ (and also CA_2) decreased, showing that there was a proceeding reaction between $C_{12}A_7$ and A/CA_2, as observed also for the samples heat treated at 1300 °C. The reaction was, however, not substantially faster at the higher T_2 of 1500 °C and was far from reaching completion. There were significant differences in the amounts of $C_{12}A_7$ in Q and FR (t_2 = 9 h) samples, with the latter containing considerably higher amounts. Now, $C_{12}A_7$ is melted at 1500 °C, so this phase must form upon cooling. The total phase assembly that exists together with the un-reactive CA_2 had a composition that had *ca.* 1 wt% more C than CA. According to the equilibrium phase diagram, at 1500 °C CA coexists with a liquid with a composition close to $C_{12}A_7$. It is, however, very probable that there exist in the samples local regions that have compositions that differ from the average composition. This explains the formation of C_3A in two FR samples. C_3A has only a few strong reflections, corresponding to a perovskite sub-cell[37] with $a' = a/4 = 3.816$ Å, while the rest are weak. The strong diagnostic reflection for C_3A at d = 2.70 Å is very close to a strong reflection of $C_{12}A_7$ at 2.68 Å and the reflection at 1.908 Å is just to the right of a set of reflections from CA at 1.92 to 1.93 Å. While larger amounts of C_3A can be detected by intensity increases at these positions, smaller amounts are more difficult to see in the presence of large amounts of the other phases. The lower contents of $C_{12}A_7$ in the Q samples can be explained if one assumes that the melt, or part of it, does not crystallize upon cooling, but forms a glass, or very badly crystallized phases, that are not detected in the films, leading to an apparent increase in the phase fractions of the other phases. This amorphous component should accordingly amount to *ca.* 5–15 wt%. The existence of an amorphous component in the quenched samples agrees with the obtained Ca_{tot} values, which are systematically lower for the quenched samples, however, not being accurate enough to serve as evidence.

The samples heat-treated at 900 °C for t_1 hours were found to contain mainly un-reacted A and C, $Ca(OH)_2$, formed by reaction of C with air, but also in addition CA. The Bragg reflections for the formed CA had clearly profiles and an intensity distribution different from CA formed at higher temperatures, indicating that it had the meta-stable orthorhombic/hexagonal modification.[8,11,12] Rough estimates of the amounts of CA formed are 2, 9 and 20 wt% for t_1 = 1, 20 and 40 h, respectively. These results show, first, that C reacts with A already at low temperatures and secondly, that the first crystalline phase to form is in fact CA.

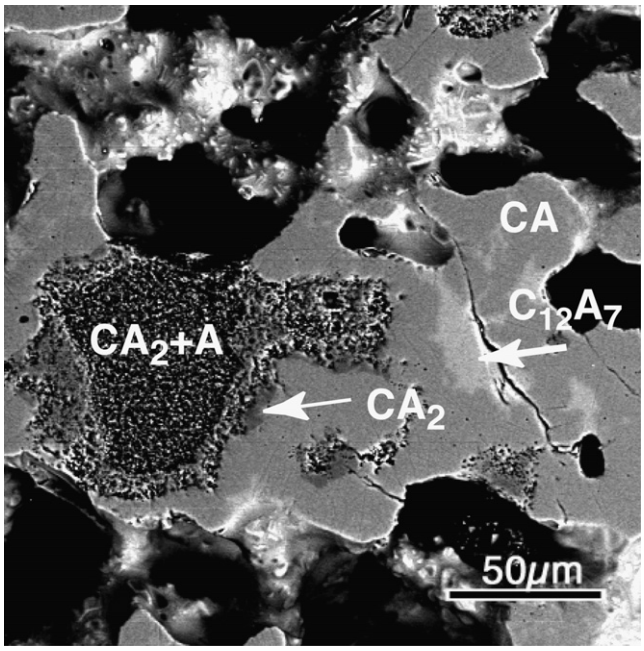

Fig. 2. BSE image of sample heat-treated at 1400 °C (t_1 = 20 h, t_2 = 4.5 h). Pores filled with plastic are seen as black regions.

3.3. Scanning electron microscopy

Back-scattered electron (BSE) images for samples heat-treated at 1400 °C (t_1 = 20 h, t_2 = 4.5 h) are shown in Fig. 2. The samples are sintered and contain inter-connected voids. The images show, as for all samples, three characteristic gray scales; darker gray, corresponding to either a mixture of A and CA_2 or solely CA_2, medium grey, corresponding to the main phase CA, and light grey, corresponding to $C_{12}A_7$. $C_{12}A_7$ is found in pockets within the main matrix of CA. A mixture of A and CA_2 is observed in porous regions of sizes ranging up to 100 μm. Surrounding these regions there is a layer of CA_2. According to XRPD, the amount of CA_2 is *ca.* 6 wt%, the amount of A *ca.* 2 wt%, and the amount of $C_{12}A_7$ ca. 15 wt%. It should be noted that it was not possible to unequivocally determine the composition from EDS-SEM as the grains were too small.

Representative images for samples heat-treated at 1300 °C for t_2 = 1 h are shown in Fig. 3. The samples are more porous due to the lower T_2. Lighter regions containing co-existing CA and $C_{12}A_7$ surround darker regions containing A and CA_2. The former two phases are intimately mixed, with grain sizes of ca. 0.3–0.5 μm. A layer of CA_2 surrounds the A/CA_2 regions. For samples heat-treated for the longer time of t_2 = 40 h, see Fig. 4, the regions containing co-existing CA and $C_{12}A_7$ have densified more and show larger pores. According to the XRPD data these samples contain less A and $C_{12}A_7$ than those with t_2 = 1 h. The more porous regions containing A and CA_2 are here also surrounded by layers of CA_2.

According to the equilibrium phase diagram, CA co-exists with a liquid phase with approximately $C_{12}A_7$ composition at 1500 °C. The corresponding samples contain, see Fig. 5, compact larger regions with CA and $C_{12}A_7$, with a total amount of *ca.* 90 wt%. The grain size of CA is here much larger, ranging up to *ca.* 100 μm, and the pockets of $C_{12}A_7$ are quite separated. In addition there are quite large voids or cavities, partly filled with porous agglomerates of CA_2 (*ca.* 7 wt%) and, less, A (*ca.* 2 wt%). The brighter BSE contrast at the rims of holes and voids imply that they contained more Ca than the surrounding matrix, consisting probably of a layer of $C_{12}A_7$. Images for samples with a longer t_2 time of 9 h were quite similar. According to XRPD, the amount of $C_{12}A_7$ (and also to a lesser extent of CA_2) is smaller, showing a comparatively slow proceeding reaction towards CA, and there is no un-reacted A left. The existence of the very large pockets with CA_2 clearly explains the slowness of the reaction. Quenched samples showed a lot of formed cracks, resulting in pull-out during polishing, but otherwise showed similar images as those from FR samples.

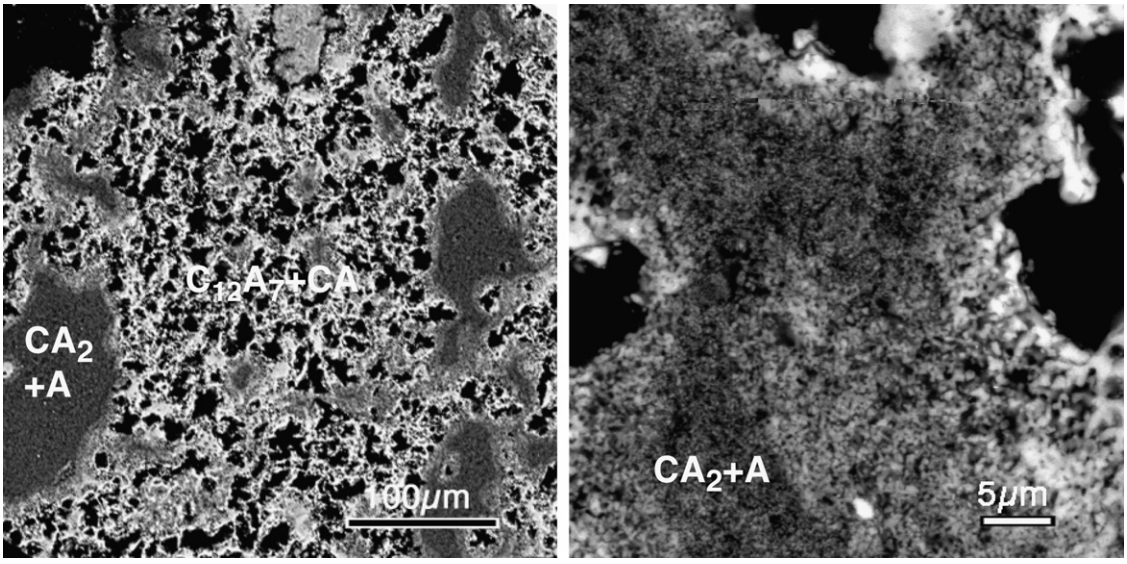

Fig. 3. BSE images of sample heat-treated at 1300 °C, t_2 = 1 h.

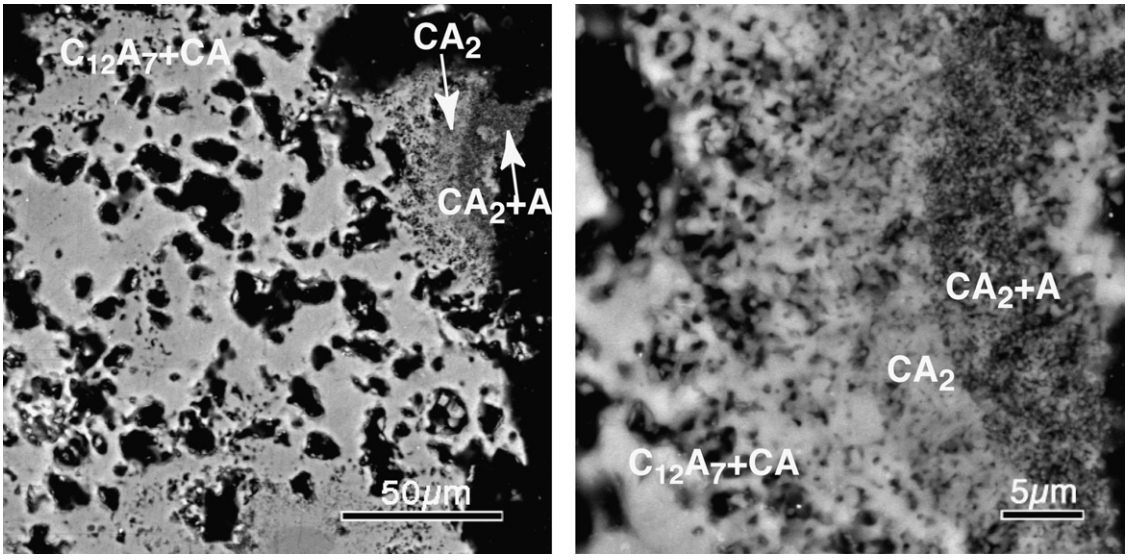

Fig. 4. BSE images of sample heat-treated at 1300 °C, $t_2 = 9$ h.

3.4. Metastable CA modification

The XRPD data for samples heat-treated at 900 °C indicated the presence CA with the meta-stable orthorhombic/hexagonal modification.[8,11,12] The structures of both the stable monoclinic and the meta-stable modification are stuffed-tridymite derivatives, consisting of frameworks of corner-shared AlO_4 tetrahedra with Ca atoms in their interstices. The stable modification is isostructural with beryllonite ($NaBePO_4$) and the low-temperature modifications of $NaMM'O_4$ (MM′ = GaSi, AlGe, GaGe).[40] The unit cell parameters are related to those of hexagonal kalsilite ($KAlSiO_4$), A and C, by $a \approx \sqrt{3}A$, $b \approx C$, $c \approx 3A$, $\beta \approx 90.3°$. The observed powder pattern of the meta-stable modification indicates that it is isostructural with the "high-temperature" modifications of $NaMM'O_4$ (MM′ = GaSi, AlGe, GaGe) reported by Barbier and Fleet[40] and $NaGaSiO_4$-I,[41] the latter a phase obtained by thermal composition of the sodalite $Na_6[GaSiO_4]_6(H_2O)_8$. Nearly all reflections in the pattern can accordingly be indexed with a hexagonal unit cell with $a = 8.732(2)$ Å and $c = 8.078(2)$ Å. No significant broadening of reflections of the type $h\,k\,0$ could furthermore be observed that could imply a lower symmetry. However, as also found in the case of $NaGaSiO_4$-I,[41] two weak reflections remain unaccounted for by this hexagonal cell, at $d = 4.73$ and 3.19 Å, with relative intensities of *ca.* 1–2%. These correspond to 112 and 114 reflections, respectively, for an orthorhombic unit cell with similar unit cell dimensions as the monoclinic unit cell for the stable modification, indicating that the space group symmetry is orthorhombic. For the $NaMM'O_4$ compounds, orthorhombic unit cells have indeed been verified by electron diffraction.[40] The crystals invariably showed twinning on the (1 3 0) and (1 1 0) planes, generating patterns with pseudo-hexagonal symmetry.

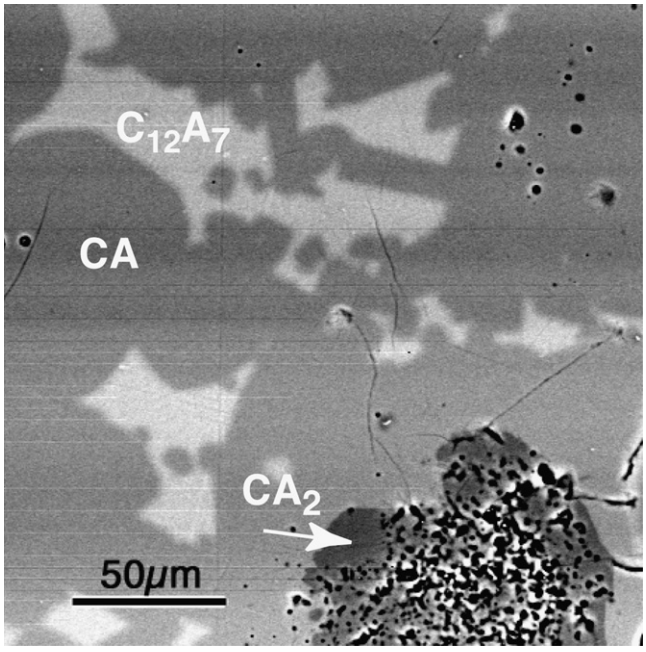

Fig. 5. BSE images of sample heat-treated at 1500 °C, $t_2 = 9$ h.

Selected area electron diffraction patterns of crystallites of the metastable modification of $CaAl_2O_4$ are shown in Fig. 6. The [0 1 0] zone axis pattern is consistent with a B-centered unit cell. Tilting the crystal around [0 0 1] reveals reflections corresponding to $c = 15.2$ Å, which excludes the hexagonal unit cell with $a = 8.73$ Å. Zone axis electron diffraction patterns recorded along [1 0 0] and [0 0 1] are also shown. The electron diffraction studies reveal that the crystallites are twinned and that streaking is present due to frequent disorder. The presence of twinning is not surprising, considering that the structure is close to hexagonal in a projection along the b axis. As a consequence of the twinning, many of the electron diffraction patterns are better described as superimpositions of two or more directions in an orthorhombic cell that are equal in the corresponding hexagonal cell. Such a twinning can only take place if a considerable disordering exists in the packing sequence along the b-axis which can explain the streaking in the diffraction pattern. Similar patterns have been reported for $NaGaGeO_4$ phases.[40]

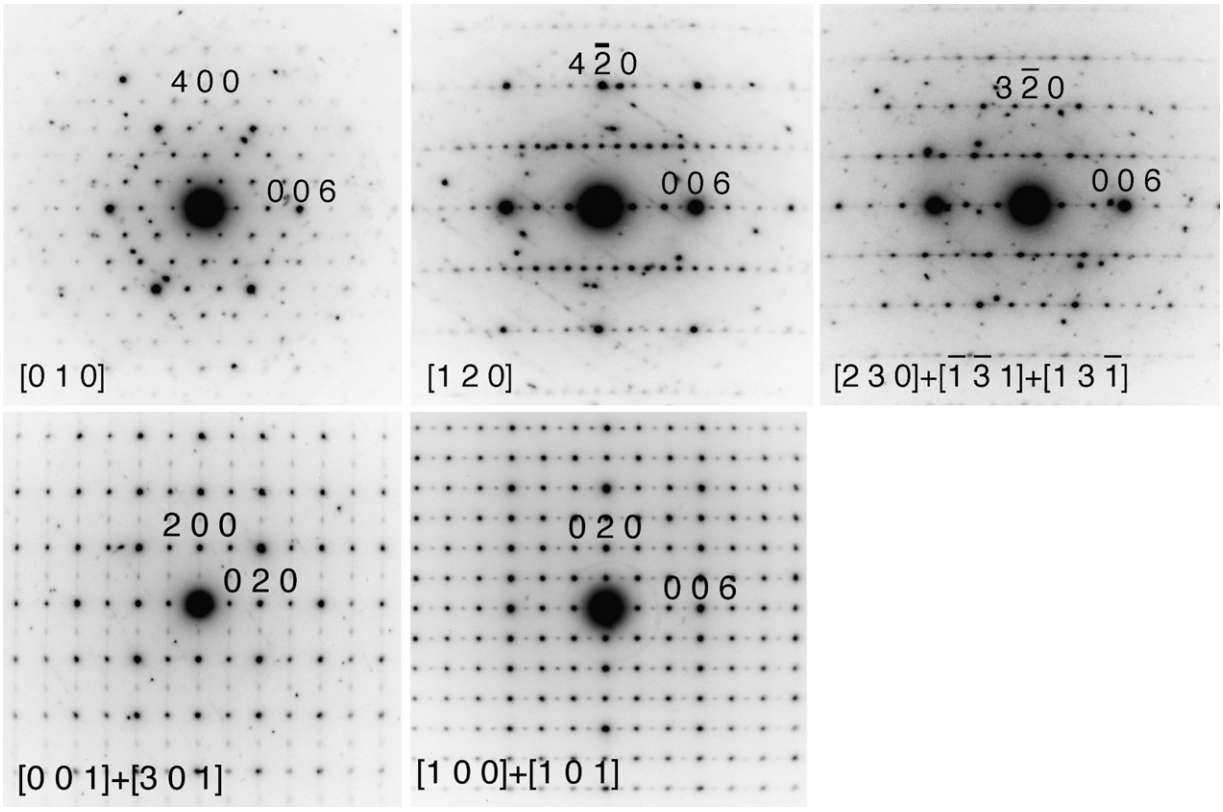

Fig. 6. Selected area electron diffraction patterns of crystallites of the metastable modification of $CaAl_2O_4$. The indexing corresponds to an orthorhombic unit cell with similar dimensions as the monoclinic cell of the stable modification. Several of the SAED patterns are superimpositions of different zone axes that are equivalent in hexagonal tridymite (given within parenthesis).

3.5. Transmission electron microscopy

The presence of a glass phase in samples quenched from 1500 °C could not be deduced with certainty by XRPD. Four selected samples was therefore crushed, put on holey carbon films, and investigated by TEM. Most crystallites had EDPs typical for crystalline phases and no crystallites where found with completely lacking Bragg reflections. However, a small number of crystallites had EDPs indicating very disordered crystallites. These crystallites could well be melted (or glass) phases that crystallize very poorly upon cooling. The composition of these "disordered crystallites" were, however, always found to be close to Ca:Al = 1:2 and not as could be expected 6:7.

Thin foils from the interfaces between the regions described above, *i.e.*: darker gray, corresponding to either a mixture of A and CA_2 or solely CA_2, medium grey, corresponding to the main phase CA, and light grey, corresponding to $C_{12}A_7$, were produced using FIB, see Fig. 7. The interfaces were very sharp with no marked diffusion gradient between the neighbouring phases; see Fig. 8, as determined from energy dispersive X-ray microanalysis.

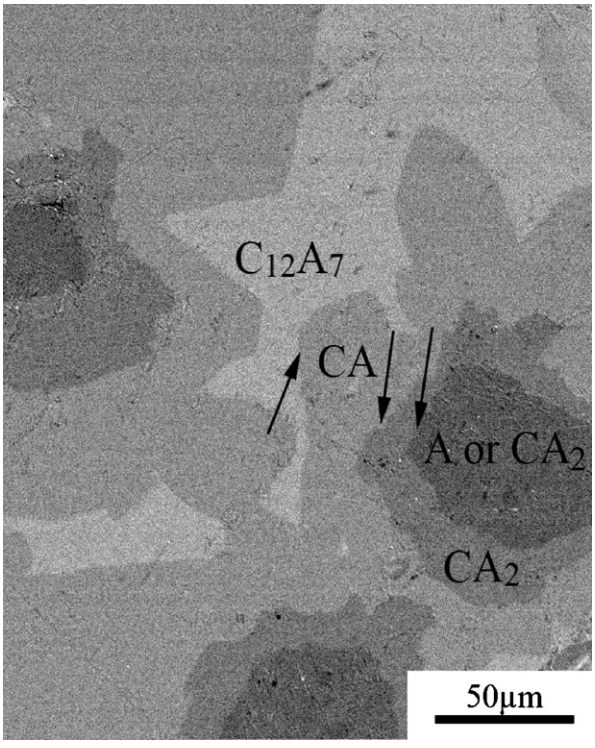

Fig. 7. Marked areas for FIB cut between the different regions of interest.

4. Discussion

In addition to CA, the heat-treated samples contained major amounts of the neighbouring phases CA_2 and $C_{12}A_7$, and in some cases also un-reacted A. Only one FR sample, treated at

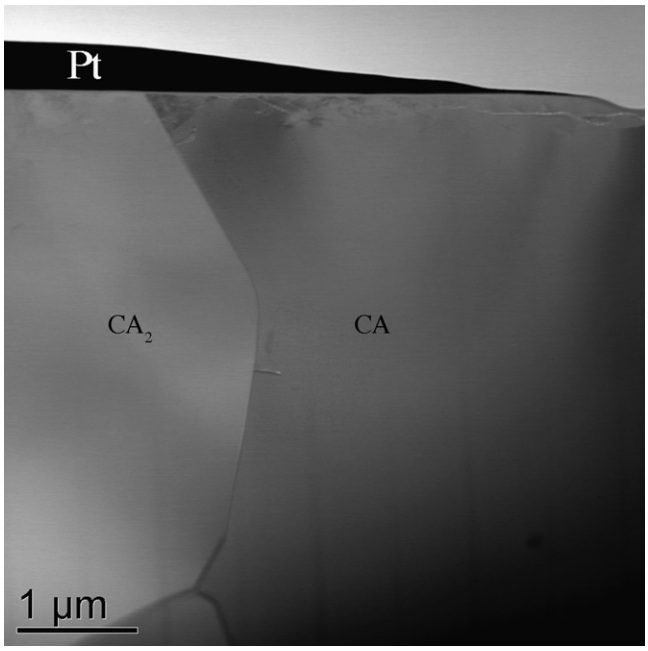

Fig. 8. Bright field STEM image from the interface between CA and CA_2.

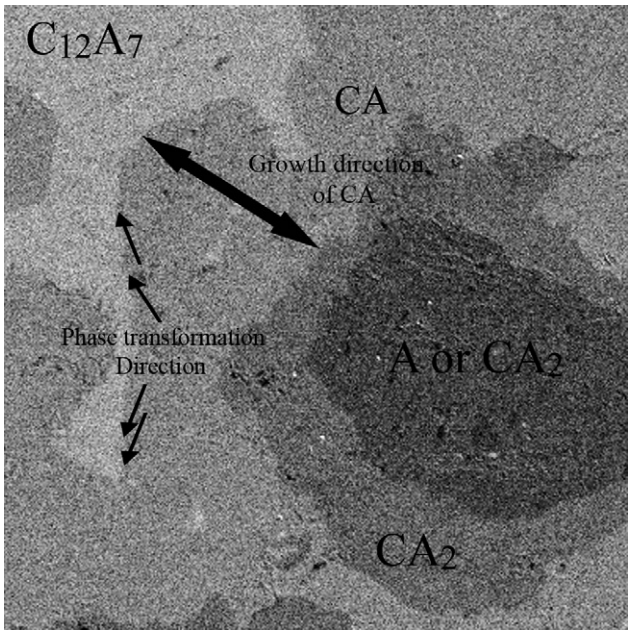

Fig. 9. BSE image illustrating the phase formation of CA. Ca is grossly diffusing inwards to the regions richer in A. The growth of the CA phase is occurring in the direction of the interfaces.

1500 °C, contained trace amounts of C_3A, most probably formed upon solidification of a liquid phase. The absence of C_3A in all other samples does to some extent not agree with previous studies.[14–16] However, the temperatures applied in these studies were in general lower and all studies suggest that C_3A forms at low temperatures and that its amount then decreases comparatively faster with time. The holding time t_1 at $T_1 = 900$ °C has no effect on phase formation at $T_2 = 1300$–1500 °C. The amount of CA increases with holding time t_2 at T_2, as the Ca-rich phase $C_{12}A_7$ reacts with A and/or CA_2 to form CA. The reaction with A has a lower Gibbs free energy (−14.3 kJ/mol CA formed) than the reaction with CA_2 (−7.1 kJ/mol CA formed)[20] and is thermodynamically thus favoured. SEM images show that a layer of CA_2 is as a rule formed around regions containing A and CA_2.

The proceeding of the reactions towards completion is slow and is not substantially faster at 1500 than 1400 °C. The SEM studies show that this is due to that, early on, porous isolated regions, with sizes up to 100 μm, containing A/CA_2 are formed within a matrix of finely inter-dispersed CA and $C_{12}A_7$. In order to reach reaction completion, Ca atoms must diffuse across large distances and react with the A/CA_2. The layer of comparatively denser CA_2 formed around the A/CA_2 regions may here also act as a diffusion barrier. The initial formation of the A/CA_2 regions is most likely due to agglomeration of A in the dry-mixed raw material. The higher Ca content at the surfaces of the pores could be an indication that the Ca-diffusion during phase formation to a large extent takes place at the surface of the grains.

Our results do not support the notion that the Ca-rich phases $C_{12}A_7$ and C_3A are formed as inter-mediate phases, while CA_2 is formed via an initial side reaction.[16] Local Ca poor regions lead to the formation of CA_2 in equilibrium with A. A single heat treatment at 1350 °C for 24 h of the mixture with CA composition that was tumbled in propanol and additionally hand-ground, in order to avoid agglomeration, yielded essentially pure (97 wt%) CA. Furthermore, the only Ca aluminate phase that formed at 900 °C is CA.

No significant differences were found between Q and FR samples heat-treated at 1300 and 1400 °C. In Q samples from 1500 °C, the amounts of CA were found smaller in comparison with FR samples. It is likely that this decrease is only apparent, and due to that poorly crystallized phases form, which are not detected by XRPD, from the liquid phase upon quenching. The TEM studies did show the presence of poorly crystallized phases. However, further studies are necessary for validation and quantification. The interface between two neighbouring phases is sharp and does not contain a detectable diffusion gradient. This means that the phase transformation occurs in the direction of the interface and not perpendicular to it. Thus the investigated regions going from $C_{12}A_7$ to A is the actual diffusion gradient for the reaction. A schematic image of the phase transformation can be seen in Fig. 9. Calcium is diffusing inwards to the regions richer in alumina. The actual phase transformation is occurring in the direction of the interface. With time the driving force for the phase transformation from CA_2 to CA slows down due to limited space for the extra alumina that forms due to the transformation, *i.e.* there need to be area in the microstructure to accommodate the extra alumina. This could be the driving force for the alumina rich cores found in the structure.

Samples heat-treated at 900 °C, show that a reaction between C and A occurs at this low temperature leading to the formation of the meta-stable orthorhombic/hexagonal modification of CA. TEM shows for the this phase EDPs that are typical for a disordered phase, with intensities clearly different from those of monoclinic CA.

The Rietveld method, using Guinier-Hägg film data, has been used in our work to determine the phase fractions of the Ca alu-

minates. The method can, in many cases, give reliable results without using standards and have been applied to phase analysis of calcium aluminate cements.[42–44] When relatively few phases are present, as here, satisfactory quantitative results can be obtained using conventional X-ray diffractometer or powder cameras.

5. Conclusions

- Holding time at low temperatures, to remove CO_2, has no effect on the phase formation at higher temperatures. CA is the only phase that forms at the low temperatures.
- The proceeding of the reactions towards completion is slow even at high temperatures.
- The microstructure forms in distinct layers going from A to $C_{12}A_7$.
- Rapid quenching from high temperature does not seem to show significant differences between samples.

Acknowledgements

Mr. L. Göthe is thanked for help with recording the Guinier-Hägg films. Göran Gustafson foundation for academic research is acknowledged for financial support.

References

1. Chatterjee, A. K. and Zhmoidin, G. I., Phase equilibrium diagram of the system calcium oxide–aluminum oxide–calcium fluoride. *J. Mater. Sci.*, 1972, **7**, 93–97.
2. Nurse, R. W., Welch, J. H. and Majumdar, A. J., The $CaO–Al_2O_3$ system in a moisture-free atmosphere. *Trans. Br. Ceram. Soc.*, 1965, **64**, 409–418.
3. Hallstedt, B., Assessment of the $CaO–Al_2O_3$ system. *J. Am. Ceram. Soc.*, 1990, **73**, 15–23.
4. Eriksson, G. and Pelton, A. D., Critical evaluation and optimization of the thermodynamic properties and phase diagrams of the $CaO–Al_2O_3$, $Al_2O_3–SiO_2$, and $CaO–Al_2O_3–SiO_2$ systems. *Metall. Trans. B*, 1993, **24B**, 807–816.
5. Vincent, M. G. and Jeffery, J. W., The crystal structure of pentacalcium trialuminate, $5CaO·3Al_2O_3$. *Acta Crystallogr. Sect. B*, 1978, **34**, 1422–1428.
6. Rog, G., Kozlowska-Rog, A., Zakula-Sokol, K. and Borchardt, G., Determination of the standard Gibbs free energies of formation of the calcium aluminates from the oxides by e.m.f. measurements. *J. Chem. Thermodyn.*, 1993, **25**, 807–810.
7. Aitasalo, T., Durygin, A., Hölsä, J., Lastusaari, M., Niitykoski, J. and Suchocki, A., Low temperature thermoluminescence properties of Eu^{2+} and R^{3+} doped $CaAl_2O_4$. *J. Alloys Compd.*, 2004, **380**, 4–8.
8. Aitasalo, T., Hölsä, J., Jungner, H., Lastusaari, M., Niitykoski, J., Parkkinen, M. and Valtonen, R., Eu^{2+}-doped calcium aluminates prepared by alternative low temperature routes. *Opt. Mat.*, 2004, **26**, 113–116.
9. Sunnegårdh-Grönberg, K., Calcium aluminate cement as dental restorative, Mechanical properties and clinical durability, Umeå University Odontological Dissertations, No. 84, ISSN 0345-7532, ISBN 91-7305-589-1, 2004.
10. Engqvist, H., Schultz-Walz, J.-E., Loof, J., Botton, G. A., Mayer, D., Phaneuf, M. W., Ahnfelt, N.-O. and Hermansson, L., Chemical and biological integration of a mouldable bioactive ceramic material capable of forming apatite in vivo in teeth. *Biomaterials*, 2004, **25**, 2781–2787.
11. Ito, S., Ikai, K., Suzuki, K. and Inagaki, M., Metastable orthorhombic calcium dialuminum tetraoxide. *J. Am. Ceram. Soc.*, 1975, **58**, 79–80.
12. Aitasalo, T., Hölsä, J., Jungner, H., Lastusaari, M. and Niitykoski, J., Comparison of sol–gel and solid-state prepared Eu^{2+} doped calcium aluminates. *J. Mater. Sci.*, 2002, **20**, 15–20.
13. Scrivener, K. and Capmas, A., In *Calcium Aluminate Cements, Lea's Chemistry of Cement and Concrete*, ed. P. C. Hewlett. Arnold, 1998.
14. Williamson, J. and Glasser, F. P., Reactions in heated lime-alumina mixtures. *J. Appl. Chem.*, 1962, **12**, 535–538.
15. Singh, V. K., Ali, M. M. and Mandal, U. K., Formation kinetics of calcium aluminates. *J. Am. Ceram. Soc.*, 1990, **73**, 872–876.
16. Mohamed, B. M. and Sharp, J. H., Kinetics and mechanism of formation of monocalcium aluminate, $CaAl_2O_4$. *J. Mater. Chem.*, 1997, **7**, 1595–1599.
17. Tas, A. C., Chemical preparation of the binary compounds in the calcia-alumina system by self-propagating combustion synthesis. *J. Am. Ceram. Soc.*, 1998, **81**, 2853–2863.
18. Fumo, D. A., Morelli, M. R. and Segadaes, A. M., Combustion synthesis of calcium aluminates. *Mat. Res. Bull.*, 1996, **31**, 1243–1255.
19. Douy, A. and Gervais, M., Crystallization of amorphous precursors in the calcia-alumina system: a differential scanning calorimetry study. *J. Am. Ceram. Soc.*, 2000, **83**, 70–76.
20. Rivas Mercury, J. M., De Aza, A. H. and Pena, P., Synthesis of $CaAl_2O_4$ from powders: Particle size effect. *J. Eur. Ceram. Soc.*, 2005, **25**, 3269.
21. Gulgun, M. A., Popoola, O. O. and Kriven, W. M., Chemical synthesis and characterization of calcium aluminate powders. *J. Am. Ceram. Soc.*, 1994, **77**, 531–539.
22. Goktas, A. A. and Weinberg, M. C., Preparation and crystallisation of sol–gel calcia-alumina compositions. *J. Am. Ceram. Soc.*, 1991, **74**, 1066–1070.
23. Pati, R. K., Panda, A. B. and Pramanik, P., Preparation of nanocrystalline calcium aluminate powders. *J. Mat. Syn. Proc.*, 2002, **10**, 157–161.
24. Uberoi, M. and Risbud, S. H., Processing of amorphous calcium aluminate powders at <900 °C. *J. Am. Ceram. Soc.*, 1990, **73**, 1768–1770.
25. Stephan, D. and Wilhelm, P., Synthesis of pure cementitious phases by sol-gel process as precursor. *Z. Anorg. Allg. Chem.*, 2004, **630**, 1477–1483.
26. Cinibulk, M. K. and Hay, R. S., Textured magnetoplumbite fiber–matrix interphase derived from sol–gel fiber coatings. *J. Am. Ceram. Soc.*, 1996, **79**, 1233–1246.
27. Singh, V. P. and Sharma, K. K., Low-temperature synthesis of calcium hexaaluminate. *J. Am. Ceram. Soc.*, 2002, **84**, 769–772.
28. Johansson, K.-E., Palm, T. and Werner, P.-E., An automatic microdensitometer for x-ray powder diffraction photographs. *J. Phys. Sect. E*, 1980, **13**, 1289–1291.
29. Werner, P. E., Eriksson, L. and Salome, S., *SCANPI, A Program for Evaluating Guinier Photographs*. Stockholm University, 1980.
30. Rodriguez-Carjaval, J., FULLPROF Version 3.2, ILL, Grenoble, March 2005.
31. Inorganic Crystal Structure Database, ICSD, Database Version 2005-2, Fachinformationszentrum Karlsruhe (FIZ), Germany.
32. Powder Diffraction File PDF-4+ 2005, International Centre for Diffraction Data (ICCD).
33. Cox, D. E., Moodenbaugh, A. R., Sleight, A. W. and Chen, H. Y., Structural refinement of neutron and x-ray data by the Rietveld method: application to Al_2O_3 and $BiVO_4$. *NBS Spec. Pub.*, 1980, **567**, 189–201.
34. Ponomarev, V. I., Kheiker, D. M. and Belov, N. V., Crystal structure of calcium dialuminate. *Kristallografiya*, 1970, **15**, 1140–1143.
35. Hoerkner, W. and Mueller-Buschbaum, H., Crystal structure of calcium aluminate ($CaAl_2O_4$). *J. Inorg. Nucl. Chem.*, 1976, **38**, 983–984.
36. Christensen, A. N., Neutron powder diffraction profile studies on $Ca_{11.3}Al_{14}O_{32.3}$ and $CaClOD(D_{0.88}H_{0.12})$. *Acta Chem Scand. A*, 1987, **41**, 110–112.
37. Mondal, P. and Jeffery, J. W., Crystal structure of tricalcium aluminate, $Ca_3Al_2O_6$. *Acta Crystallogr. Sect. B*, 1975, **31**, 689–697.
38. Langford, R. M. and Petford-Long, A. K., Preparation of transmission electron microscopy cross-section specimens using focused ion beam milling. *J. Vac. Sci. Technol. A*, 2001, **19**, 2186–2193.
39. Phaneuf, M. W., Applications of focused ion beam microscopy to material science specimens. *Micron*, 1999, **30**, 277.
40. Barbier, J. and Fleet, M. E., Investigation of structural states in the series $MGaSiO_4$, $MAlGeO_4$, $MGaGeO_4$ (M = sodium, potassium). *J. Solid State Chem.*, 1987, **71**, 361–370.

41. Gesing, Th. M., Structure and properties of tecto-gallosilicates. I. Hydrosodalites and their phase transition. *Z. Kristallogr.*, 2000, **215**, 510–517.
42. Guirado, F. and Gali, S., Quantitative Rietveld analysis of CAC clinker phases using synchrotron radiation. *Cem. Concr. Res.*, 2006, **36**, 2021–2032.
43. Füllmann, T., Walenta, G., Bier, T., Espinosa, B. and Scrivener, K. L., Quantitative Rietveld analysis of calcium aluminate cements. *World Cement*, 1999, **30**, 91–96.
44. Guirado, F., Gali, S. and Chinchón, S., Quantitative Rietveld analysis of aluminous cement clinker phases. *Cem. Concr. Res.*, 2000, **30**, 1023–1029.